



## Article

# Enhancement of Sensitivity with High–Reflective–Index Guided–Wave Nanomaterials for a Long–Range Surface Plasmon Resonance Sensor

Leiming Wu <sup>1,2,3</sup> , Kai Che <sup>4</sup>, Yuanjiang Xiang <sup>5,\*</sup> and Yuwen Qin <sup>1,2,3,\*</sup>

<sup>1</sup> Institute of Advanced Photonics Technology, School of Information Engineering, Guangdong University of Technology, Guangzhou 510006, China; leiming\_wu@gdut.edu.cn

<sup>2</sup> Guangdong Provincial Key Laboratory of Information Photonics Technology, Guangdong University of Technology, Guangzhou 510006, China

<sup>3</sup> Southern Marine Science and Engineering Guangdong Laboratory (Zhuhai), Zhuhai 519000, China

<sup>4</sup> Department of Electrical and Information Engineering, Hubei University of Automotive Technology, Shiyan 442002, China; 20160010@huat.edu.cn

<sup>5</sup> School of Physics and Electronics, Hunan University, Changsha 410082, China

\* Correspondence: xiang78@hnu.edu.cn (Y.X.); qinyw@gdut.edu.cn (Y.Q.)

**Abstract:** A guided–wave long–range surface plasmon resonance (GW–LRSPR) sensor was proposed in this investigation. In the proposed sensor, high–refractive–index (RI) dielectric films (i.e., CH<sub>3</sub>NH<sub>3</sub>PbBr<sub>3</sub> perovskite, silicon) served as the guided–wave (GW) layer, which was combined with the long–range surface plasmon resonance (LRSPR) structure to form the GW–LRSPR sensing structure. The theoretical results based on the transfer matrix method (TMM) demonstrated that the LRSPR signal was enhanced by the additional high–RI GW layer, which was called the GW–LRSPR signal. The achieved GW–LRSPR signal had a strong ability to perceive the analyte. By optimizing the low– and high–RI dielectrics in the GW–LRSPR sensing structure, we obtained the highest sensitivity (S) of 1340.4 RIU<sup>−1</sup> based on a CH<sub>3</sub>NH<sub>3</sub>PbBr<sub>3</sub> GW layer, and the corresponding figure of merit (FOM) was 8.16 × 10<sup>4</sup> RIU<sup>−1</sup> deg<sup>−1</sup>. Compared with the conventional LRSPR sensor (S = 688.9 RIU<sup>−1</sup>), the sensitivity of this new type of sensor was improved by nearly 94%.

**Keywords:** long–range surface plasmon resonance; high–refractive–index guided–wave layer; sensitivity



**Citation:** Wu, L.; Che, K.; Xiang, Y.; Qin, Y. Enhancement of Sensitivity with High–Reflective–Index Guided–Wave Nanomaterials for a Long–Range Surface Plasmon Resonance Sensor. *Nanomaterials* **2022**, *12*, 168. <https://doi.org/10.3390/nano12010168>

Academic Editors: Marcin Runowski and Weichun Huang

Received: 30 November 2021

Accepted: 31 December 2021

Published: 4 January 2022

**Publisher's Note:** MDPI stays neutral with regard to jurisdictional claims in published maps and institutional affiliations.



**Copyright:** © 2022 by the authors. Licensee MDPI, Basel, Switzerland. This article is an open access article distributed under the terms and conditions of the Creative Commons Attribution (CC BY) license (<https://creativecommons.org/licenses/by/4.0/>).

## 1. Introduction

The Kretschmann–Raether (KR) configuration [1] is an important carrier for the excitation of the surface plasmon resonance (SPR) phenomenon [2–4]. Metals, such as gold (Au), silver (Ag), aluminum (Al), and copper (Cu), contain a large number of free electrons on their surface. These free electrons oscillate up and down in the direction perpendicular to the surface of the metal film under the excitation of TM–polarized light, thereby forming a surface plasmon wave (SPW). When the evanescent wave generated by the attenuated total reflection of the incident light matches the SPW, they will resonate and form a resonance signal. The resonance signal allows for sensitive detection that is used as the principle of designing sensors. The SPR sensors are widely applied in environmental monitoring [5,6], biochemical reactions [7,8], medical diagnosis [9,10], and other fields. Sreekanth et al. [11] proposed a hyperbolic metamaterials–based plasmonic biosensor with a high sensitivity of 30,000 nm per RIU, which can detect ultralow–molecular–weight (244 Da) biomolecules at picomolar concentrations. Garol et al. [12] reported a nanoporous gold metamaterials–based plasmonic sensor, where the sensitivity was demonstrated to be 15,000 nm per RIU. Kabashin et al. [13] used plasmonic nanorod metamaterials to design a biosensor, where the sensitivity was more than 30,000 nm per RIU. Moreover, the plasmonic nanorod metamaterials can also be applied in high–pressure sensors [14,15], as well as

surface-enhanced Raman scattering (SERS) [16]. Runowski et al. [14] reported that gold nanorods can be used as a high-pressure sensor to effectively detect phase transitions of compressed compounds. Chiang et al. [15] proposed a compact plasmonic metal-insulator-metal pressure sensor that the maximum sensitivity was as high as 592.44 nm/MPa.

In the SPR configuration, Au is usually selected as the metal layer for exciting SPR because of its strong oxidation resistance. In the resonance signal, there are many sensitive variables, such as the intensity of the reflectance [17,18], the resonance angle [19,20], and the phase [21,22], which can be used to track and detect a change in the sensing analyte. The SPR signal generated by the Au film has a strong detection ability for the analyte close to the sensing interface. However, the detection ability will gradually decay as the detection depth increases. The detection depth of the conventional SPR sensor is generally less than 200 nm [23], which makes it difficult to effectively detect some macromolecules with a diameter of several hundred nanometers. In order to solve this defect, LRSPR [24,25] is used as a detection signal to improve the detection depth of the sensor. In the LRSPR configuration, the metal layer is thin enough so that the upper and lower SPWs of the metal film are coupled together, thereby enhancing the electric field at the sensing interface. A previous report [26] indicated that the detection depth of the LRSPR sensor can exceed 1  $\mu\text{m}$ , which greatly improves the sensor's ability to detect analytes. Compared with an SPR sensing structure, LRSPR has many advantages [24,27]: (1) stronger electric field intensity, (2) deeper detection distance, (3) narrower resonance detection signal, and (4) higher detection accuracy. In addition to the LRSPR sensor, some other novel sensors were also reported with high performance, such as a plasmonic photonic crystal fiber sensor [28], plasmonic nanorod sensor [29], metal-insulator-metal (MIM) sensor [30], monolithic metal dimer-on-film-structure-based sensor [31], and toroidal-metadevices-based sensor [32]. These innovative sensing structures have all contributed to improving the performance of plasmonic sensors.

In order to improve the sensitivity, a sensing structure, named guided-wave SPR (GWSPR), was proposed, which enhances the sensitivity of conventional sensors by adding an additional GW layer [33,34]. The result demonstrates that the sensitivity of the SPR sensor is improved by one order of magnitude with an additional GW layer. However, the additional GW layer greatly enhances the electric field intensity but does not contribute to the increase of the detection depth. Therefore, in order to enhance the sensitivity and increase the detection depth, a novel sandwich layer of a metal-dielectric-structure-based plasmonic sensor is proposed. TMM, which is a method that is widely used in the design of sensing structures, was used as the theoretical method to investigate the performance of the proposed GW-RSPR sensor. It was found that the resonance signal of the LRSPR configuration was enhanced by an additional high-RI GW layer, which greatly improved the electric field intensity, as well as the sensitivity, and retained the ability of the LRSPR sensor to detect a large depth. With such excellent performance, the GW-LRSPR sensing structure is promising for applications in biosensing, chemical sensing, and optical sensing.

## 2. Design Consideration and Numerical Model

The configuration of an LRSPR sensor is composed of a sandwich structure made up of a low-RI layer/metal film/low-RI layer (Figure 1a). In this study, a GW-LRSPR sensing structure made up of a prism/low-RI dielectric/high-RI dielectric/Au/sensing analyte was proposed. In our investigation, cytop was selected as the low-RI dielectric layer near the side of the prism, which has a low RI of 1.34. In addition to cytop, other low-RI materials, such as LiF and  $\text{MgF}_2$ , are also widely used in the design of LRSPR sensors with high sensitivity [20]. The low-RI layer on the other side of the LRSPR configuration was the sensing analyte, and its RI was  $n_s = 1.33 + \Delta n_s$ . Here,  $\Delta n_s$  represents the slight change in the sensing analyte, where this change could be a biological action or a chemical reaction. In the sandwich structure, Au was used as the metal layer to excite the long-range surface

plasma waves due to its good oxidation resistance. The RI of Au is expressed by the Drude–Lorentz model as follows [35]:

$$n_{Au} = \left( 1 - \frac{\lambda^2 \lambda_C}{\lambda_p^2 (\lambda_C + i\lambda)} \right)^{1/2} \quad (1)$$

where  $\lambda = 633$  nm,  $\lambda_C = 8.9342 \times 10^{-6}$  m, and  $\lambda_p = 1.6826 \times 10^{-7}$  m. In addition, BK7, SF10, and 2S2G ( $\text{Ge}_{20}\text{Ga}_5\text{Sb}_{10}\text{S}_{65}$ ) were used as coupling prisms in the sensing structure. Their refractive indices are defined as:

$$n_{BK7} = \left( \frac{1.03961212\lambda^2}{\lambda^2 - 0.00600069867} + \frac{0.231792344\lambda^2}{\lambda^2 - 0.0200179144} + \frac{1.03961212\lambda^2}{\lambda^2 - 103.560653} + 1 \right)^{1/2} \quad (2)$$

for the BK7 prism,

$$n_{SF10} = \left( \frac{1.62153902\lambda^2}{\lambda^2 - 0.0122241457} + \frac{0.256287842\lambda^2}{\lambda^2 - 0.0595736775} + \frac{1.64447552\lambda^2}{\lambda^2 - 147.468793} + 1 \right)^{1/2} \quad (3)$$

for the SF10 prism, and

$$n_{2S2G} = 2.24047 + \frac{2.693 \times 10^{-2}}{\lambda^2} + \frac{8.08 \times 10^{-3}}{\lambda^4} \quad (4)$$

for the 2S2G prism. When the wavelength of incident light is 633 nm, the RI of the BK7, SF10, and 2S2G prisms are 1.5151, 1.723, and 2.358, respectively. To improve the sensitivity of the LRSPR sensor, we considered inserting a GW material with high RI between the Au film and the low-RI dielectric layer to form a GW–LRSPR sensing structure (Figure 1b). The GW material (high-RI dielectric film) was  $\text{CH}_3\text{NH}_3\text{PbBr}_3$  perovskite, where its RI is  $2 + 0.003i$  at  $\lambda = 633$  nm [36,37]. The parameters optimization of the sensing structure is discussed in Section 3 “Results.” The results showed that the optimal thicknesses of the low-RI dielectric, high-RI dielectric, and Au film were 2430 nm, 4 nm, and 10 nm, respectively.

In the proposed sensor, the low-RI dielectric film was cytop, which is widely used in sensing applications and can be deposited on the cover glass using evaporation. Thereafter, the high-RI dielectric film of perovskite could be transferred to the surface of the cytop using a self-assembly method. Next, the gold film was sprayed onto the surface of the high-RI dielectric film by the method of magnetic co-sputtering. Finally, the cover glass and the prism were glued together with the matching liquid to prepare the proposed sensing structure. The sensing process was divided into three steps: first, fasten the sample cell tightly on the surface of the sensing structure; second, use a pump to control the analyte so that it flows slowly through the sample cell; finally, use the resonance signal to detect the analyte flowing through the sample cell.

In a multi-layer sensing structure, the transfer matrix method (TMM) [38,39] is usually used as the theoretical method to study the performance of a proposed plasmon sensor. The simulation software used was Matlab. Each layer in the multi-layer structure can be expressed as a matrix:

$$M_k = \begin{bmatrix} \cos \beta_k & (-i \sin \beta_k) / q_k \\ -iq_k \sin \beta_k & \cos \beta_k \end{bmatrix} \quad (5)$$

where  $\beta_k = \frac{2\pi d_k}{\lambda} (\varepsilon_k - n_1^2 \sin^2 \theta)^{1/2}$  and  $q_k = \frac{(\varepsilon_k - n_1^2 \sin^2 \theta)^{1/2}}{\varepsilon_k}$ . Here,  $d_k$  is the thickness of each layer in the multilayer sensing structure,  $\varepsilon_k$  is the dielectric constant of each layer, and  $n_1$  is the RI of the prism. The characteristic transfer matrix of the sensing configuration is as follows:

$$M = \prod_{k=2}^{N-1} M_k = \begin{bmatrix} M_{11} & M_{12} \\ M_{21} & M_{22} \end{bmatrix} \quad (6)$$

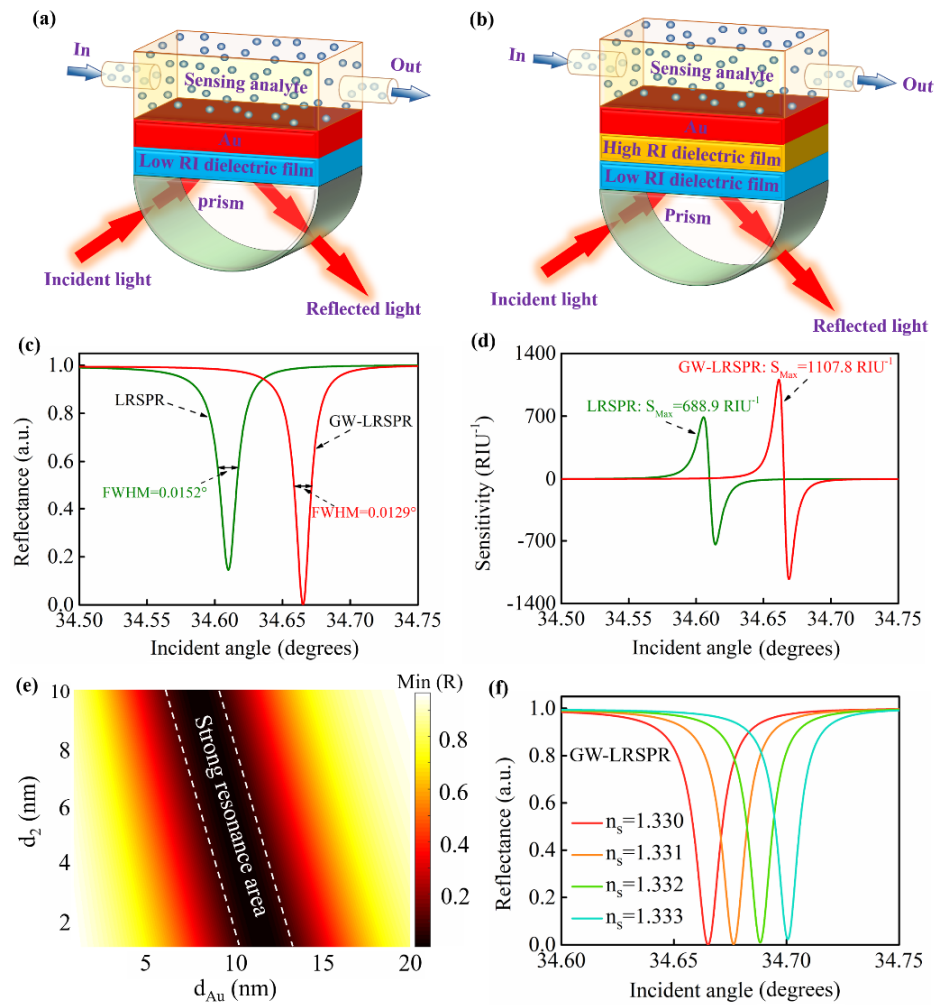


**Figure 1.** (a) Schematic diagram of the 10 nm thick Au–based conventional long–range surface plasmon resonance sensor. (b) Schematic diagram of the proposed high–RI–dielectric film–based GW–LRSR sensor. (c) The resonance signals generated from the LRSR and GW–LRSR sensors based on the 2S2G prism, where their full width at half maximum (*FWHMs*) were 0.0152° and 0.0129°, respectively. (d) The sensitivities of the conventional Au–based LRSR sensor and the novel GW–LRSR sensor. (e) The strong resonance area of the proposed GW–LRSR sensor at different  $d_2$  and  $d_{Au}$  values. (f) The curves of reflectance excited from the GW–LRSR sensor when  $n_s$  ranged from 1.330 to 1.333. Note: the results of Figure c–f were obtained from the LRSR and GW–LRSR configurations based on the 2S2G prism.

The reflectance of the multilayer sensing structure is given as:

$$R = |r_p|^2 = \left| \frac{(M_{11} + M_{12}q_N)q_1 - (M_{21} + M_{22}q_N)}{(M_{11} + M_{12}q_N)q_1 + (M_{21} + M_{22}q_N)} \right|^2 \quad (7)$$

The intensity sensitivity (*S*) and figure of merit (*FOM*) are expressed as:

$$S = \frac{\Delta R}{\Delta n_s} \quad (8)$$

and

$$FOM = \frac{S}{FWHM} \quad (9)$$

where  $FWHM$  is the full width at half maximum and  $\Delta R$  is the intensity change of the reflectance curve caused by the change in the sensing analyte ( $\Delta n_s$ ). In our numerical calculations,  $\Delta n_s$  represents a slight change in the sensing medium and was set to 0.0001.

### 3. Results

The resonance signals excited from the configuration of the LRSR and GW–LRSR are shown in Figure 1c, which indicates that an additional high–RI GW layer ( $\text{CH}_3\text{NH}_3\text{PbBr}_3$  perovskite) could improve the quality of the resonance signal. We first calculated the maximum loss and then calculated half of its maximum. At the half–maximum point on the SPR curve, two different angle values were obtained. Then, by subtracting the lesser angle from the greater angle, the difference obtained was the  $FWHM$ . The result demonstrated that the GW–LRSR had a narrower  $FWHM$  and a deeper resonance dip than that of the LRSR. In contrast, the resonance signal of the GW–LRSR was stronger than that of the LRSR. According to Equation (8), the corresponding intensity sensitivities of the LRSR and GW–LRSR were calculated using the TMM (Figure 1b). The result showed that the GW–LRSR sensor had a higher sensitivity than that of the LRSR sensor due to the enhancement of the resonance signal by the GW layer. After adding the GW layer, the sensitivity of the LRSR sensor increased from  $688.9 \text{ RIU}^{-1}$  to  $1107.8 \text{ RIU}^{-1}$ . Furthermore, the  $FWHM$  of the resonance signal became narrower after adding the GW layer, which promoted the improvement of the FOM according to Equation (9). The FOM of the LRSR sensor was  $4.53 \times 10^4 \text{ RIU}^{-1} \text{ deg}^{-1}$ , which was improved to be  $8.58 \times 10^4 \text{ RIU}^{-1} \text{ deg}^{-1}$  after adding a high–RI GW layer to form the GW–LRSR configuration. For the resonance signals, the stronger the resonance, the deeper the dip. In the GW–LRSR sensor, the thickness of both the high–RI dielectric and Au film had a great influence on the resonance signal. The area between the two white curves in Figure 1e is the strong resonance region of the proposed sensor at different  $d_2$  and  $d_{\text{Au}}$  values. Therefore, in the design of the sensing structure, the selection of the thickness of both the high–RI dielectric and Au film needed to correspond to the strong resonance region. Figure 1f shows the detection result of the resonance signal on the change in the RI of the sensing analyte based on the GW–LRSR sensor. It was found that the resonance signal was sensitive to the change in RI, and it gradually moved to a larger angle as the RI of the sensing analyte increased.

In order to clearly demonstrate the enhancement of the high–RI GW layer on the sensitivity of the LRSR sensor, the electric field distribution comparison between the LRSR and GW–LRSR is discussed. The electric field distribution curves of the LRSR and GW–LRSR at their resonance angles are shown in Figure 2. The results of the comparison showed that the electric field intensity of the sensor structure was improved by the additional high–RI GW layer. The enhancement of the electric field at the sensing interface improved the sensor's ability to perceive changes in the sensing medium, thereby increasing the sensitivity of the sensor.

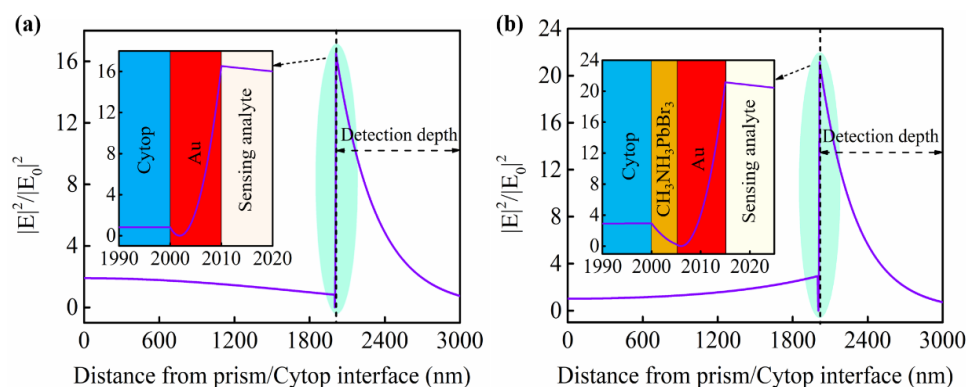


**Figure 2.** The electric field distribution of the plasmon sensors based on (a) LRSR and (b) GW–LRSR at the resonance angle ( $\theta_{res} = 34.6100^\circ$  for LRSR,  $\theta_{res} = 34.6652^\circ$  for GW–LRSR).

There are four approaches for calculating the sensitivity of a sensor [23], including intensity sensitivity, angular sensitivity, spectral sensitivity, and phase sensitivity. For angular sensitivity, a previous report demonstrated that the selection of coupling prism has a great impact on the performance of the sensor [19]. Therefore, it is necessary to analyze the influence of the coupling prism on the sensitivity of the proposed GW–LRSPR sensor. Herein, the intensity sensitivity was used to calculate and analyze the performance of the proposed sensor, which is different from the angular sensitivity. Figure 3a,b shows the reflectance and intensity sensitivity for the proposed GW–LRSPR sensor based on SF10 and BK7, respectively. The intensity sensitivity for the SF10–based GW–LRSPR sensor was  $1131.2 \text{ RIU}^{-1}$  (Figure 3a), while the intensity sensitivity for the BK7–based GW–LRSPR sensor was  $1030.1 \text{ RIU}^{-1}$  (Figure 3b). These results were similar to the intensity sensitivity of the 2S2G–based sensor shown in Figure 1d,f. Assuming that the RI of the prism was variable, the intensity sensitivities of the proposed GW–LRSPR sensor under different prisms were calculated and are shown in Figure 3c. The results demonstrated that the coupling prism with different RIs had little effect on the intensity sensitivity of the proposed GW–LRSPR sensor. Therefore, 2S2G, SF10, and BK7 can all be used as coupling prisms in the proposed GW–LRSPR sensor, and will not have a significant impact on intensity sensitivity. According to Snell's law, a change in the RI of the prism will lead to a change in the critical angle of total reflection. With the increase in the RI of the prism, the critical angle of total reflection will gradually decrease; therefore, the resonance signal will also move toward the direction of a small angle. In this process, the characteristics of the resonance signal were basically unchanged and the sensitivity changed slightly.

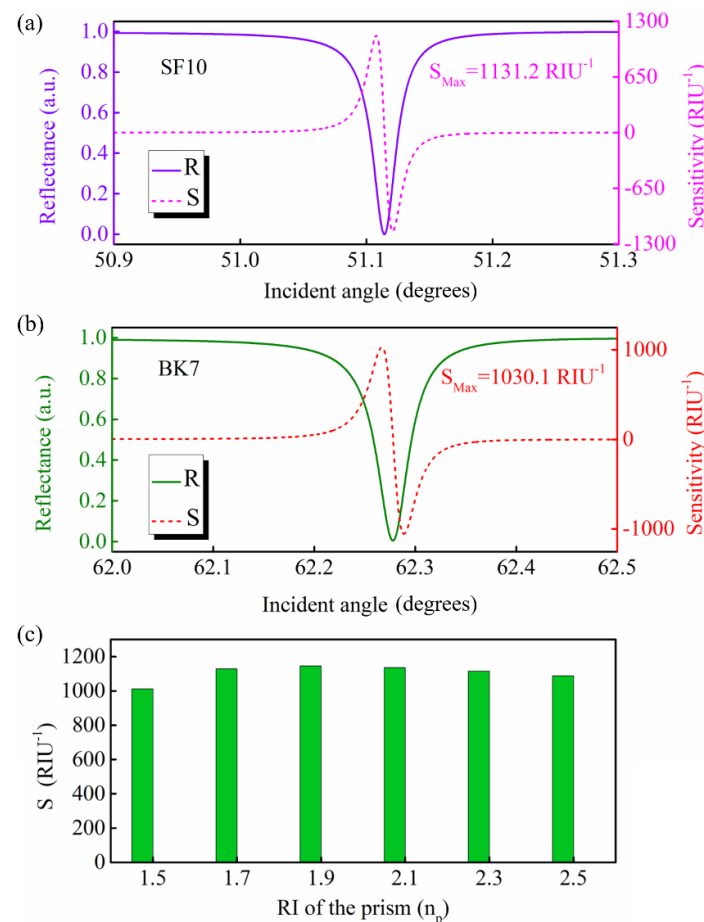


**Figure 3.** Reflectance and sensitivity of the proposed GW–LRSPR sensor based on (a) SF10 and (b) BK7 prisms. (c) The sensitivity of the proposed GW–LRSPR sensor based on different prisms.

For the following discussion, the SF10 was selected as the coupling prism in the sensing structure. After completing the selection of the coupling prism, we optimized the thickness of the low-RI dielectric layer and the high-RI GW layer to obtain the optimal sensing sensitivity. The enhancement mechanism is that the surface plasmon on the metal surface is allowed to be transmitted to the high-RI GW film, thereby enhancing the electric field at the sensing interface. When the high-RI GW film is thin enough, most of the evanescent field is located in the analyte area, increasing the detection range and sensitivity [33]. Figure 4a shows the intensity sensitivity as a function of the thickness of the low-RI dielectric film ( $d_1$ ). When the  $d_1$  ranged from 1000 nm to 3800 nm, the intensity sensitivity gradually increased first and reached its maximum value of  $S_{\text{Max}} = 1326.6 \text{ RIU}^{-1}$  at  $d_1 = 2430 \text{ nm}$ . The FOM corresponding to the maximum sensitivity was  $8.1 \times 10^4 \text{ RIU}^{-1} \text{ deg}^{-1}$ . Furthermore, when  $n_1$  changed from 1.33 to 1.36, the corresponding sensitivity also changed, and a greater sensitivity could be obtained in the range of 1.33 to 1.34 (Figure 4b). Therefore, the cytop material, which has an  $n_1$  of 1.34, was selected as the low-RI dielectric film, and the thickness was defined as 2430 nm in the proposed GW-LRSPR sensor. Additionally, the thickness of the high-RI GW layer was also an important parameter to optimize the performance of the GW-LRSPR sensor. Figure 4c shows the resonance signals excited from the proposed GW-LRSPR sensor at different  $d_2$  values. The corresponding intensity sensitivity and FOM were achieved and are shown in Figure 4d. The result showed that the highest sensitivity ( $S = 1340.4 \text{ RIU}^{-1}$ ) was obtained at  $d_2 = 4 \text{ nm}$ , with FOM =  $8.16 \times 10^4 \text{ RIU}^{-1} \text{ deg}^{-1}$ . Therefore, in order to maintain a high sensitivity ( $S > 1200 \text{ RIU}^{-1}$ ) for the proposed GW-LRSPR sensor, the allowable thickness variation range for the high-RI dielectric film was 2100 nm to 2800 nm, and the allowable thickness variation range for the low-RI dielectric film was 2 nm to 6 nm.

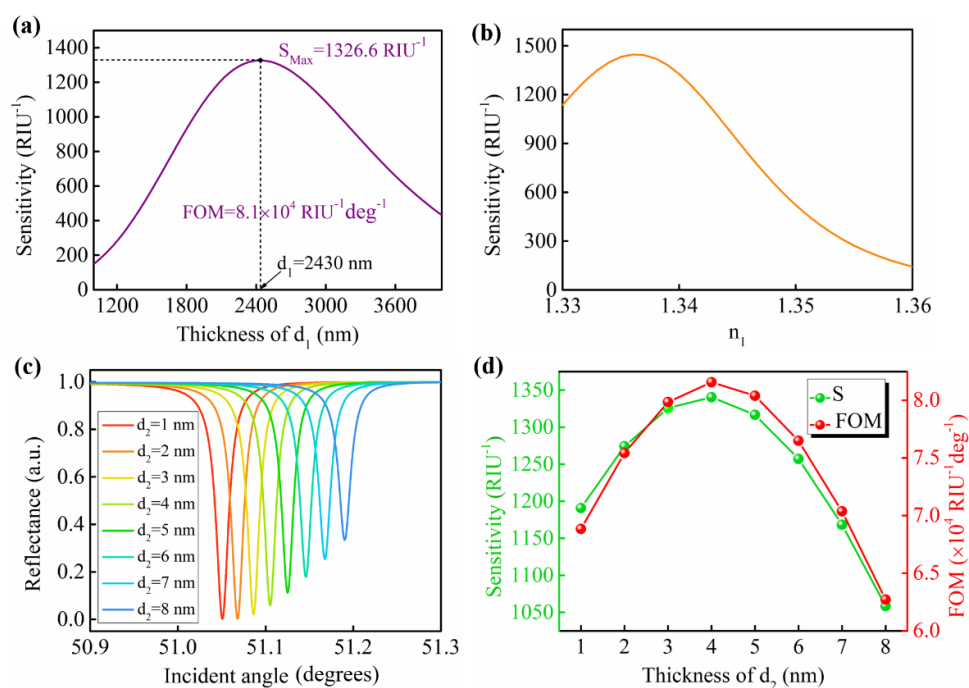


**Figure 4.** (a) Variation of the intensity sensitivity when the thickness of the low-RI dielectric film ( $d_1$ ) ranged from 1000 nm to 3800 nm for the proposed GW-LRSPR sensor. (b) The intensity sensitivity as a function of the RI of the low-RI dielectric film ( $n_1$ ) at  $d_1 = 2430 \text{ nm}$ . (c) The reflectance curves of the proposed GW-LRSPR sensor at different thicknesses of the low-RI GW layer ( $d_2$ ) when  $d_1 = 2430 \text{ nm}$  and  $n_1 = 1.34$ . (d) The intensity sensitivity and FOM of the GW-LRSPR sensor at different  $d_2$  values.

The resonance signal excited from the GW-LRSPR sensor was sensitive to the change in RI in the sensing analyte. A slight change in the sensing analyte can cause an obvious

shift in the resonance angle (Figure 5a). When the RI of the sensing analyte changed from 1.32 to 1.345, the FWHM of the resonance signal became narrower and narrower (Figure 5b). After calculations, the results showed that the intensity sensitivity of the GW–LRSPR sensor increased to the highest value ( $S = 1533.7 \text{ RIU}^{-1}$ ) at  $n_s = 1.334$  and then gradually decreased (Figure 5c). Furthermore, the FOM of the GW–LRSPR sensor continued to increase in the range of  $n_s = 1.32 \sim 1.345$  and reach the maximum value ( $\text{FOM} = 11.45 \times 10^4 \text{ RIU}^{-1} \text{ deg}^{-1}$ ) at  $n_s = 1.337$  (Figure 5d).

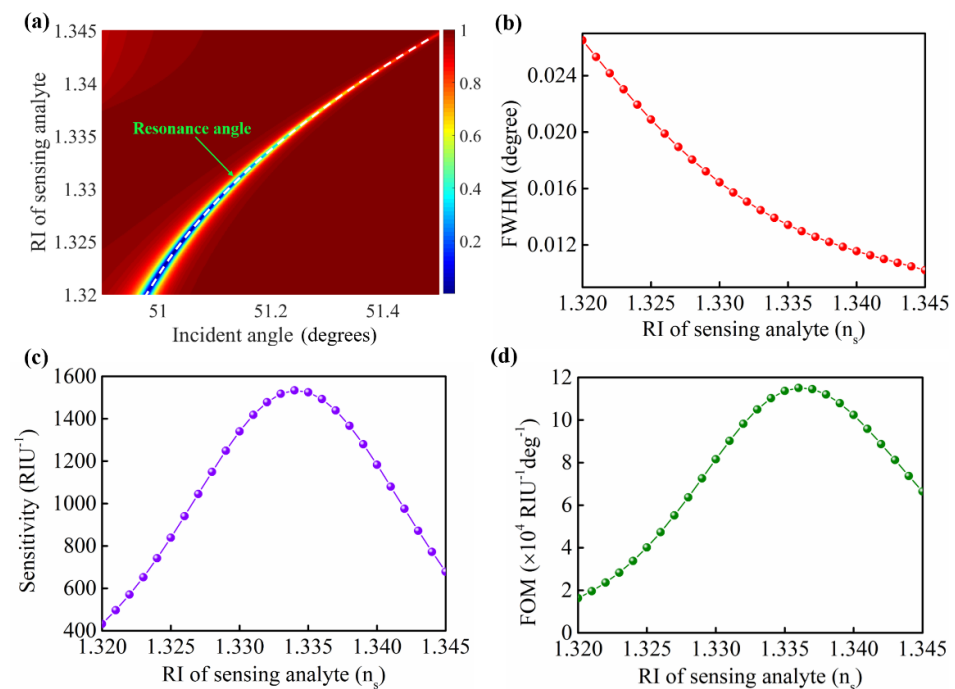


**Figure 5.** (a) The resonance angle shift caused by the RI change of the sensing analyte. (b) The FWHM of the resonance signal under different RIs of the sensing analytes. (c) The intensity sensitivity of the proposed GW–LRSPR sensor with different  $n_s$  values. (d) The FOM of the proposed GW–LRSPR sensor with different  $n_s$  values.

In addition to  $\text{CH}_3\text{NH}_3\text{PbBr}_3$  perovskite, other high–RI dielectrics can also be used as GW layers to improve the sensing sensitivity of an LRSPR sensor. Figure 6a shows the intensity sensitivity optimized by  $n_2$  and  $d_2$ . The result indicated that the GW dielectrics with different high RIs could achieve higher sensitivities in the appropriate thickness range. Herein, silicon was exemplified as another high–RI GW layer to enhance the sensitivity of the GW–LRSPR sensor. The resonance signal and intensity sensitivity of the GW–LRSPR sensor with a 3 nm thick silicon GW layer is shown in Figure 6b. The result demonstrated that high sensitivity of  $1392.3 \text{ RIU}^{-1}$  could be obtained when the GW layer was silicon. The above results demonstrated that the silicon–f the sensing analyte changed from 1.330 to 1.335, the corresponding resonance signal moved significantly (Figure 6c).

Furthermore, the sensitivity of the proposed GW–LRSPR sensor could also be calculated in terms of the spectral sensitivity ( $S = \Delta\lambda/\Delta n_s$ ). When the  $n_s$  changed from 1.33 to 1.3301 ( $\Delta n_s = 0.0001$ ), the spectral sensitivity was calculated to be  $7097 \text{ nm/RIU}$ . The variation in the resonance signal with respect to the wavelength is shown in Figure 7a. It was found that the proposed sensor was sensitive to the change in  $n_s$ , and even if the  $n_s$  had a change of only 0.0001, it could still be effectively detected. The spectral sensitivity and FOM under different  $n_s$  values are shown in Figure 7b. When the  $n_s$  increased from 1.33 to 1.34, both the  $S$  and FOM changed accordingly. After calculations, the highest spectral sensitivities could be obtained as  $7285 \text{ nm/RIU}$  at  $n_s = 1.335$ . Such excellent performance means that the GW–LRSPR sensing structure can play an active role in many fields, including environmental monitoring, medical diagnosis, and biological testing.

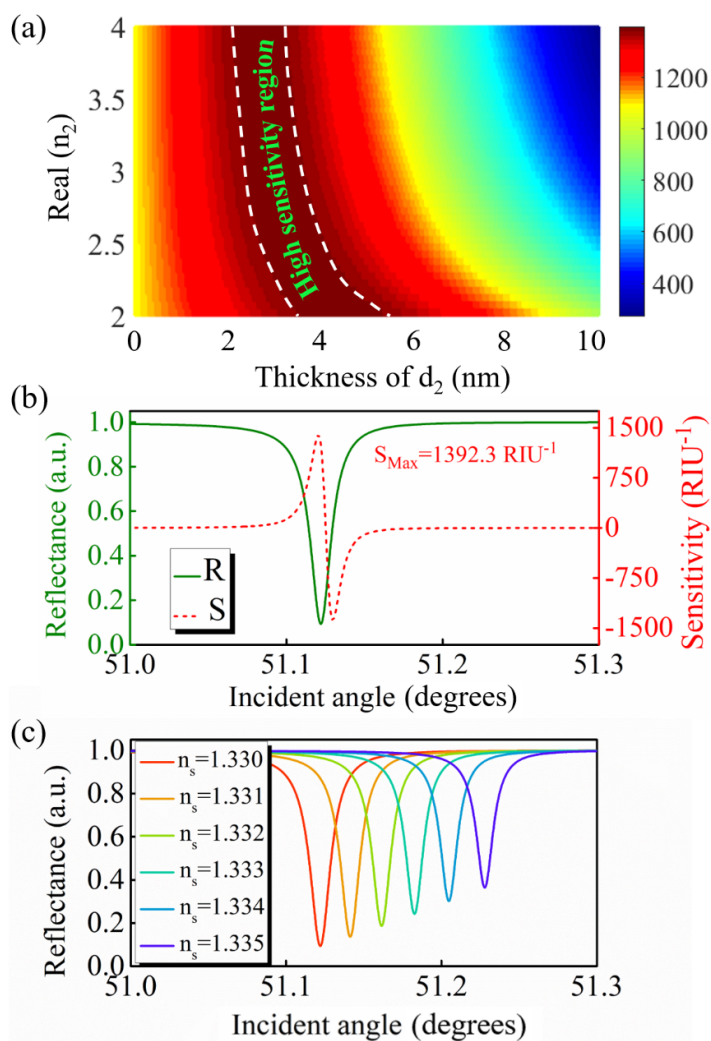


**Figure 6.** (a) Optimizing  $n_2$  and  $d_2$  to obtain the highest sensitivity. (b) The resonance signal of the proposed GW–LRSPR sensor and its corresponding sensitivity at  $d_2 = 3$  nm when the high–RI GW layer was silicon. (c) Shift of the resonance signal at different RIs of the sensing analytes.

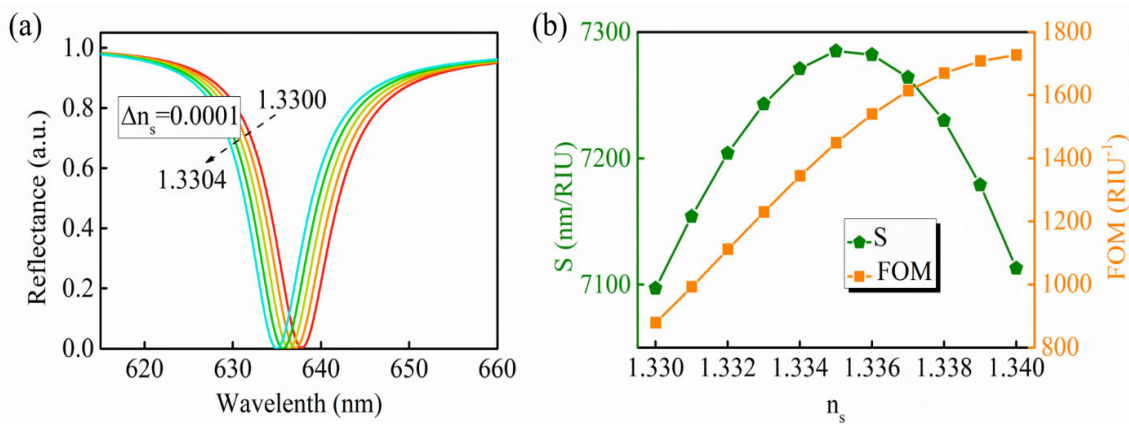


**Figure 7.** (a) The variation of the resonance signal with respect to the wavelength when the  $n_s$  ranged from 1.33 to 1.3304 ( $\Delta n_s = 0.0001$ ). (b) The spectral sensitivity ( $S = \Delta\lambda/\Delta n_s$ ) and the corresponding FOM of the proposed GW–LRSPR based on silicon. Note: the incident angle was fixed at  $51.12^\circ$ .

#### 4. Conclusions

In this study, a high-RI GW layer (i.e.,  $\text{CH}_3\text{NH}_3\text{PbBr}_3$  perovskite, silicon) was combined with an LRSPR structure to form the proposed GW-LRSPR sensing structure. It was found that the resonance signal of the LRSPR structure was enhanced by the additional high-RI GW layer. When the GW layer was introduced into the LRSPR structure, the electric field at the sensing interface was effectively enhanced, thereby improving the sensing ability of the sensor. By optimizing the GW-LRSPR sensing structure, the maximum sensitivity ( $1340.4 \text{ RIU}^{-1}$ ) was obtained with the GW layer of the  $\text{CH}_3\text{NH}_3\text{PbBr}_3$  perovskite, and the corresponding FOM was  $8.16 \times 10^4 \text{ RIU}^{-1} \text{ deg}^{-1}$ . The GW-LRSPR sensor was sensitive to the change in the sensing analyte. When the RI of the sensing analyte was 1.334, a high sensitivity of  $S = 1533.7 \text{ RIU}^{-1}$  could be obtained. Moreover, another high-RI GW layer of silicon could also be used to improve the sensing sensitivity in the GW-LRSPR structure. The result showed that adding a 3 nm thick silicon guide-wave layer could increase the sensitivity to  $1392.3 \text{ RIU}^{-1}$ .

**Author Contributions:** Conceptualization, Y.X. and Y.Q.; methodology, Y.Q. and L.W.; software, K.C. and L.W.; validation, L.W., Y.X. and Y.Q.; investigation, L.W. and K.C.; resources, Y.Q.; data curation, L.W.; writing—original draft preparation, L.W.; writing—review and editing, Y.X. and Y.Q.; supervision, Y.X.; project administration, Y.Q.; funding acquisition, Y.X. and Y.Q. All authors have read and agreed to the published version of the manuscript.

**Funding:** This work is partially supported by the National Key R&D Program of China (grant no. 2018YFB1801001), the Southern Marine Science and Engineering Guangdong Laboratory (Zhuhai), the National Natural Science Foundation of China (grant no. 62105069), the Postdoctoral Research Foundation of China (grant no. 402210053), the Guangdong Introducing Innovative and Entrepreneurial Teams of “The Pearl River Talent Recruitment Program” (grant no. 2019ZT08  $\times$  340), the Research and Development Plan in Key Areas of Guangdong Province (grant no. 2018B010114002), the Guangdong Provincial Key Laboratory of Information Photonics Technology (grant no. 2020B121201011), and the Science and Technology Planning Project of Shenzhen Municipality (JCYJ20190808143801672, JCYJ20190808150803580, and JCYJ20180508152903208).

**Data Availability Statement:** The data presented in this study are available on request from the corresponding author.

**Conflicts of Interest:** The authors declare no conflict of interest.

#### References

1. Kretschmann, E.; Raether, H. Notizen: Radiative Decay of Non Radiative Surface Plasmons Excited by Light. *Z. Nat. A* **1968**, *23*, 2135–2136. [[CrossRef](#)]
2. Liu, C.; Wang, J.; Wang, F.; Su, W.; Yang, L.; Lv, J.; Fu, G.; Li, X.; Liu, Q.; Sun, T.; et al. Surface plasmon resonance (SPR) infrared sensor based on D-shape photonic crystal fibers with ITO coatings. *Opt. Commun.* **2020**, *464*, 125496. [[CrossRef](#)]
3. Amirjani, A.; Haghshenas, D.F. Ag nanostructures as the surface plasmon resonance (SPR) high-RI sensors: A mechanistic study with an emphasis on heavy metallic ions detection. *Sens. Actuators B* **2018**, *273*, 1768–1779. [[CrossRef](#)]
4. Takemura, K. Surface Plasmon Resonance (SPR)- and Localized SPR (LSPR)-Based Virus Sensing Systems: Optical Vibration of Nano- and Micro-Metallic Materials for the Development of Next-Generation Virus Detection Technology. *Biosensors* **2021**, *11*, 250. [[CrossRef](#)] [[PubMed](#)]
5. Brulé, T.; Granger, G.; Bukar, N.; Deschênes-Rancourt, C.; Havard, T.; Schmitzer, A.R.; Martel, R.; Masson, J.-F. A field-deployed surface plasmon resonance (SPR) sensor for RDX quantification in environmental waters. *Analyst* **2017**, *142*, 2161–2168. [[CrossRef](#)]
6. Daniyal, W.; Fen, Y.W.; Fauzi, N.I.M.; Hashim, H.S.; Ramdzan, N.S.M.; Omar, N.A.S. Recent advances in surface plasmon resonance optical sensors for potential application in environmental monitoring. *Sens. Mater.* **2020**, *32*, 4191–4200. [[CrossRef](#)]
7. Jebelli, A.; Oroojalian, F.; Fathi, F.; Mokhtarzadeh, A.; Guardia, M.D.L. Recent advances in surface plasmon resonance biosensors for microRNAs detection. *Biosens. Bioelectron.* **2020**, *169*, 112599. [[CrossRef](#)]
8. Jia, S.; Bian, C.; Sun, J.; Tong, J.; Xia, S. A wavelength-modulated localized surface plasmon resonance (LSPR) optical fiber sensor for sensitive detection of mercury(II) ion by gold nanoparticles-DNA conjugates. *Biosens. Bioelectron.* **2018**, *114*, 15–21. [[CrossRef](#)]
9. Rezabakhsh, A.; Rahbarghazi, R.; Fathi, F. Surface plasmon resonance biosensors for detection of Alzheimer’s biomarkers; an effective step in early and accurate diagnosis. *Biosens. Bioelectron.* **2020**, *167*, 112511. [[CrossRef](#)]
10. Yeung, W.K.; Li, H.-F.; Chung, C.-L.; Lee, K.-L.; Wei, P.-K.; Lin, H.; Chen, H.-H.; Cheng, J.-Y. Promising urinary miRNA biomarkers t-SPR profiling for urothelial cell carcinoma. *Sens. Actuators B* **2020**, *322*, 128605. [[CrossRef](#)]

11. Sreekanth, K.V.; Alapan, Y.; ElKabbash, M.; Ilker, E.; Hinczewski, M.; Gurkan, U.A.; De Luca, A.; Strangi, G. Extreme sensitivity biosensing platform based on hyperbolic metamaterials. *Nat. Mater.* **2016**, *15*, 621–627. [[CrossRef](#)]
12. Garoli, D.; Calandrini, E.; Giovannini, G.; Hubarevich, A.; Caligiuri, V.; De Angelis, F. Nanoporous gold metamaterials for high sensitivity plasmonic sensing. *Nanoscale Horiz.* **2019**, *4*, 1153–1157. [[CrossRef](#)]
13. Kabashin, A.V.; Evans, P.; Pastkovsky, S.; Hendren, W.; Wurtz, G.A.; Atkinson, R.; Pollard, R.; Podolskiy, V.A.; Zayats, A.V. Plasmonic nanorod metamaterials for biosensing. *Nat. Mater.* **2009**, *8*, 867–871. [[CrossRef](#)]
14. Runowski, M.; Sobczak, S.; Marciniak, J.; Bukalska, I.; Lis, S.; Katrusiak, A. Gold nanorods as a high-pressure sensor of phase transitions and refractive-index gauge. *Nanoscale* **2019**, *11*, 8718–8726. [[CrossRef](#)]
15. Chou Chao, C.-T.; Chou Chau, Y.-F.; Chen, S.-H.; Huang, H.J.; Lim, C.M.; Kooch, M.R.; Thotagamuge, R.; Chiang, H.-P. Ultrahigh Sensitivity of a Plasmonic Pressure Sensor with a Compact Size. *Nanomaterials* **2021**, *11*, 3147. [[CrossRef](#)]
16. Skwierczyńska, M.; Woźny, P.; Runowski, M.; Kulpiński, P.; Lis, S. Optically active plasmonic cellulose fibers based on Au nanorods for SERS applications. *Carbohydr. Polym.* **2022**, *279*, 119010. [[CrossRef](#)]
17. Wu, L.; Guo, J.; Xu, H.; Dai, X.; Xiang, Y. Ultrasensitive biosensors based on long-range surface plasmon polariton and dielectric waveguide modes. *Photonics Res.* **2016**, *4*, 262–266. [[CrossRef](#)]
18. Wu, L.; Ling, Z.; Jiang, L.; Guo, J.; Dai, X.; Xiang, Y.; Fan, D. Long-Range Surface Plasmon With Graphene for Enhancing the Sensitivity and Detection Accuracy of Biosensor. *IEEE Photonics J.* **2016**, *8*, 4801409. [[CrossRef](#)]
19. Wu, L.; Jia, Y.; Jiang, L.; Guo, J.; Dai, X.; Xiang, Y.; Fan, D. Sensitivity Improved SPR Biosensor Based on the MoS<sub>2</sub>/Graphene–Aluminum Hybrid Structure. *J. Lightwave Technol.* **2017**, *35*, 82–87. [[CrossRef](#)]
20. Paliwal, A.; Tomar, M.; Gupta, V. Refractive Index Sensor Using Long-Range Surface Plasmon Resonance with Prism Coupler. *Plasmonics* **2019**, *14*, 375–381. [[CrossRef](#)]
21. Zeng, S.; Hu, S.; Xia, J.; Anderson, T.; Dinh, X.-Q.; Meng, X.-M.; Coquet, P.; Yong, K.-T. Graphene–MoS<sub>2</sub> hybrid nanostructures enhanced surface plasmon resonance biosensors. *Sens. Actuators B* **2015**, *207*, 801–810. [[CrossRef](#)]
22. Sreekanth, K.V.; Zeng, S.; Yong, K.-T.; Yu, T. Sensitivity enhanced biosensor using graphenehigh-RI one-dimensional photonic crystal. *Sens. Actuators B* **2013**, *182*, 424–428. [[CrossRef](#)]
23. Shalabney, A.; Abdulhalim, I. Sensitivity-enhancement methods for surface plasmon sensors. *Laser Photonics Rev.* **2011**, *5*, 571–606. [[CrossRef](#)]
24. Jing, J.-Y.; Wang, Q.; Zhao, W.-M.; Wang, B.-T. Long-range surface plasmon resonance and its sensing applications: A review. *Opt. Laser. Eng.* **2019**, *112*, 103–118. [[CrossRef](#)]
25. Zhao, X.; Zhang, X.; Zhu, X.-S.; Shi, Y.-W. Long-range surface plasmon resonance sensor based on the GK570/Ag coated hollow fiber with an asymmetric layer structure. *Opt. Express* **2019**, *27*, 9550–9560. [[CrossRef](#)]
26. Liu, Y.; Xu, S.; Xuyang, X.; Zhao, B.; Xu, W. Long-Range Surface Plasmon Field-Enhanced Raman Scattering Spectroscopy Based on Evanescent Field Excitation. *J. Phys. Chem. Lett.* **2011**, *2*, 2218–2222. [[CrossRef](#)]
27. Isaacs, S.; Abdulhalim, I. Long range surface plasmon resonance with ultra-high penetration depth for self-referenced sensing and ultra-low detection limit using diverging beam approach. *Appl. Phys. Lett.* **2015**, *106*, 193701. [[CrossRef](#)]
28. Paul, A.K. Design and analysis of photonic crystal fiber plasmonic refractive Index sensor for condition monitoring of transformer oil. *OSA Contin.* **2020**, *3*, 2253–2263. [[CrossRef](#)]
29. Chou Chau, Y.-F.; Chen, K.-H.; Chiang, H.-P.; Lim, C.M.; Huang, H.J.; Lai, C.-H.; Kumara, N.T.R.N. Fabrication and Characterization of a Metallic–Dielectric Nanorod Array by Nanosphere Lithography for Plasmonic Sensing Application. *Nanomaterials* **2019**, *9*, 1691. [[CrossRef](#)]
30. Tathfif, I.; Yaseer, A.A.; Rashid, K.S.; Sagor, R.H. Metal-insulator-metal waveguidehigh-RI optical pressure sensor embedded with arrays of silver nanorods. *Opt. Express* **2021**, *29*, 32365–32376. [[CrossRef](#)]
31. Gerislioglu, B.; Dong, L.; Ahmadivand, A.; Hu, H.; Nordlander, P.; Halas, N.J. Monolithic Metal Dimer-on-Film Structure: New Plasmonic Properties Introduced by the Underlying Metal. *Nano Lett.* **2020**, *20*, 2087–2093. [[CrossRef](#)]
32. Ahmadivand, A.; Gerislioglu, B.; Ahuja, R.; Kumar Mishra, Y. Terahertz plasmonics: The rise of toroidal metadevices towards immunobiosensings. *Mater. Today* **2020**, *32*, 108–130. [[CrossRef](#)]
33. Lahav, A.; Auslender, M.; Abdulhalim, I. Sensitivity enhancement of guided-wave surface-plasmon resonance sensors. *Opt. Lett.* **2008**, *33*, 2539–2541. [[CrossRef](#)]
34. Shalabney, A.; Abdulhalim, I. Figure-of-merit enhancement of surface plasmon resonance sensors in the spectral interrogation. *Opt. Lett.* **2012**, *37*, 1175–1177. [[CrossRef](#)]
35. Verma, R.; Gupta, B.D.; Jha, R. Sensitivity enhancement of a surface plasmon resonance based biomolecules sensor using graphene and silicon layers. *Sens. Actuators B* **2011**, *160*, 623–631. [[CrossRef](#)]
36. Britzman, S.; Garnett, E.C. Measuring n and k at the Microscale in Single Crystals of CH<sub>3</sub>NH<sub>3</sub>PbBr<sub>3</sub> Perovskite. *J. Phys. Chem. C* **2016**, *120*, 616–620. [[CrossRef](#)]
37. Wu, L.; Xiang, Y.; Qin, Y. Lossy-mode-resonance sensor based on perovskite nanomaterial with high sensitivity. *Opt. Express* **2021**, *29*, 17602–17612. [[CrossRef](#)]
38. Hansen, W.N. Electric Fields Produced by the Propagation of Plane Coherent Electromagnetic Radiation in a Stratified Medium. *J. Opt. Soc. Am.* **1968**, *58*, 380–390. [[CrossRef](#)]
39. Maharana, P.K.; Jha, R.; Palei, S. Sensitivity enhancement by air mediated graphene multilayer based surface plasmon resonance biosensor for near infrared. *Sens. Actuators B* **2014**, *190*, 494–501. [[CrossRef](#)]